DOI: 10.1002/anie.201002820

Nanomedicine

Multifunctional Gold Nanoshells on Silica Nanorattles: A Platform for the Combination of Photothermal Therapy and Chemotherapy with Low Systemic Toxicity**

*Huiyu Liu, Dong Chen, Linlin Li, Tianlong Liu, Longfei Tan, Xiaoli Wu, and Fangqiong Tang**

Plasmonic nanomaterials, especially those that can convert near-infrared (NIR) light into heat, have been developed as photothermal agents for localized hyperthermia cancer therapy. After Halas's research group first applied a coating of gold nanoshells on solid silica spheres for tumor ablation,[1] a series of NIR-light-absorbing plasmonic nanomaterials have been fabricated to kill tumorigenic cells without damaging normal cells, such as gold nanorods (GNRs),[2] gold nanocages,[3] Au_xAg_{1-x} dendrites,[4] gold nanoshells on polystyrene spheres,[5] assembled gold nanoparticles,[6] and many multifunctional nanocomposites.[7]

Based on the attractive photothermal property of these plasmonic nanomaterials to optimize cancer therapy and achieve enhanced antitumor efficacy, the combination of hyperthermia and chemotherapeutic agents is an encouraging approach, which can result in synergistic effects that are greater than the two treatments alone. GNRs were reported as producing heat to augment the toxicity of chemotherapeutic agents.[8] But by simply mixing GNRs and chemotherapeutic agents, the synergistic effects of thermo-chemotherapy are difficult to realize in vivo because co-delivery of chemotherapeutic agents together with precious GNR-induced hyperthermia sources to the target tissues is still challenging. Importantly, even though different multifunctional systems based on NIR-absorbing nanomaterials have been designed,[7] many parameters of these systems were only assessed in vitro in cellular systems, while no in vivo study of the thermo-chemotherapy effect of plasmonic nanomaterials based on gold nanoshells has been carried out. In vivo experiments on an applicable medicine system should be tested with emphasis on the antitumor effect and toxicity evaluation as they move closer to the clinical setting.

In the work reported herein, we first explored the ablation of hepatocellular carcinomas both in vivo and in vitro by the combination of photothermal therapy and chemotherapy using a multifunctional gold nanoshell. Unlike the gold nanoshell employed in the study of Halas and co-workers, the gold nanoshell we use consists of a thin gold nanoshell and a monodispersed mesoporous silica nanorattle (SN) core. SNs, synthesized by our new reported method,[9] endow gold nanoshells with many advantages through their unique structure with movable cores and mesoporous shells. They were considered as an intelligent drug-delivery system because of their high thermal, chemical, and mechanical stability, large specific surface volume, controllable mesoporous pores, and good biocompatibility. Their positively charged surface simplifies the gold nanoshell coating process by not requiring a modification step with silane coupling agents (e.g., 3-aminopropyltriethoxysilane) as in other reports.[10] Based on these advantages, gold nanoshells on silica nanorattles (GSNs) have compact gold shells, controlled uniform size, tunable optical property as NIR-light-absorbing agents, and high-payload sustained drug release as a drug-delivery system. In vitro and in vivo studies prove that the synergistic effects of GSNs for the efficacious treatment of hepatocellular carcinomas are better than the chemotherapy or photothermal therapy alone. Systematic toxicity study indicates the good biocompatibility of this kind of multifunctional gold nanoshell. Additionally, organic dye molecules can be conjugated on the gold nanoshell for imaging, thus rendering the obtained GSNs an all-in-one processing system for photothermal therapy, drug delivery, and cell imaging with low systemic toxicity.

Figure 1a shows the structure of SNs synthesized by our previous method.[9] A drug-loaded structure comprising a PEGylated (PEG = polyethylene glycol) gold nanoshell on silica nanorattle spheres (termed pGSNs) is shown in Figure 1b. The products obtained after each synthetic step are shown in Figure 1c–f. SNs have a narrow size distribution with a hydrodynamic diameter of 120 nm (see Figure 1c, and Figure S1 and Table S1 in the Supporting Information) and a positively charged surface at about 36.5 eV (Figure S2 in the Supporting Information). X-ray photoelectron spectroscopy (XPS) proves the existence of free amino groups on the SNs' surface (Figure 1g). By simply stirring for 2 hours, gold seed

[*] Dr. H. Liu, Dr. L. Li, Dr. T. Liu, L. Tan, X. Wu, Prof. F. Tang
Laboratory of Controllable Preparation and Application of Nanomaterials, Technical Institute of Physics and Chemistry
Chinese Academy of Sciences
Beijing 100190 (P. R. China)
Fax: (+86) 108-254-3521
E-mail: tangfq@mail.ipc.ac.cn
Homepage: http://nanocontrol.ipc.ac.cn
D. Chen
Beijing Creative Nanophase Hi-Tech Co. Ltd.
Beijing 100086 (P. R. China)
L. Tan
Graduate University of the Chinese Academy of Sciences
Beijing 100049 (P. R. China)

[**] We thank Prof. Jing Liu for use of the infrared thermal mapping apparatus. This work was supported by the National Hi-Tech Research and Development Program (863 Program) of China (Nos. 2009AA03z322, 2007AA021802, and 2007AA021803) and the National Natural Science Foundation of China (Nos. 60736001, 30800258, and 20873171).

Supporting information for this article is available on the WWW under http://dx.doi.org/10.1002/anie.201002820.

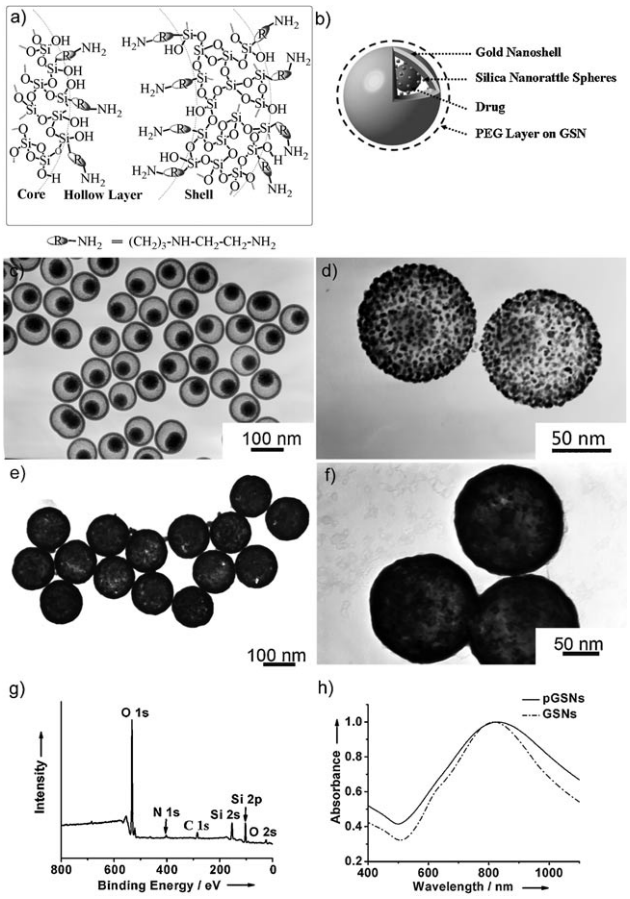

Figure 1. a) Structure of the SN. b) The drug-loaded pGSN. c–f) TEM images of c) SNs, d) gold seeds attached to SNs, e) GSNs, and f) PEGylated GSNs. g) XPS spectrum of SNs. h) Extinction spectra of GSNs and pGSNs.

nanoparticles of size 1–3 nm can be easily attached to SNs (Figure 1 d). Gold shells were grown on these SNs with attached gold seeds by further reduction of chloroauric acid, which resulted in GSNs (Figure 1 e).

Figure 1 f represents the pGSNs modified by methoxy-PEG-thiol (mPEG-SH, 5 kD) to prevent aggregation and decrease immunogenicity for in vivo application. This PEGylation resulted in a moderate increase in the average hydrodynamic diameter of GSNs from 148 to 159 nm, a size compatible with long blood residency and permeation into tumors through their leaky vasculature (Figure S1 and Table S1 in the Supporting Information). The surface plasmon resonance (SPR) band of GSNs can be tuned from the visible region of gold nanospheres to the NIR region, an optical transparency window, whereas biological tissue and water absorb minimally. The extinction spectra of pGSNs and GSNs are shown in Figure 1 h. The GSNs have a SPR peak at 815 nm, which redshifts to 824 nm after PEGylation. This redshift is due to the higher refractive index of the PEG layer relative to H_2O.

Plasmons offer a powerful means of confining light to metal/dielectric interfaces, which in turn can generate intense local electromagnetic fields and convert the laser light into ambient heat.[11] As reported, gold nanoshells possess absorption cross sections that are six orders of magnitude larger than those of some organic dyes, which makes them a much stronger NIR absorber and therefore an effective photothermal coupling agent.[12] Figure 2 shows the infrared

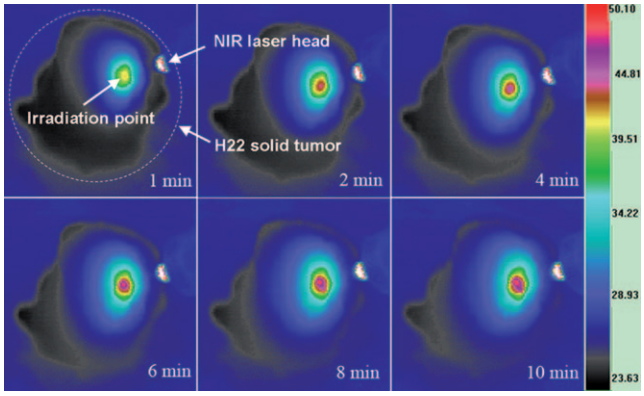

Figure 2. Infrared thermal images of an excised pGSNs-injected H22 solid tumor sample at different time points under NIR laser irradiation. The colored bar represents the relative temperature values in °C. The dashed circle indicates the H22 solid tumor.

thermal images of an excised pGSNs-injected tumor sample of hepatoma 22 (H22) under 2 $W\,cm^{-2}$ NIR laser irradiation. Before irradiation, the excised tumor was injected with pGSNs in phosphate-buffered saline (PBS) solution (200 μL, 1 $mg\,mL^{-1}$). During this irradiation, the temperature of the H22 tumor obviously increased from approximately 24 to 50 °C in the focal region as a result of the electron–phonon and phonon–phonon process of the NIR-absorbing pGSNs.[13] A comparative study of an H22 tumor sample without injection of pGSNs is shown in Figure S4 in the Supporting Information. In 10 minutes, no obvious temperature variation was observed. This proves that pGSNs are promising as an ideal photothermal converter in cancer therapy.

Another advantage of GSNs is their sustained drug-release property. SNs are advantageous for drug delivery because of their mesoporous and hollow structure. Since the GSNs were synthesized by a seed growth method and did not have ideal complete shells, the drug molecule could be released from the SNs through the openness of the shells. Figure S5 in the Supporting Information shows the cumulative docetaxel (DOC) release profiles from pGSNs in PBS buffer (pH 7.4). DOC is known to be an effective anticancer drug, but it has been difficult to give patients an adequate dose without negative side effects. The amount of DOC loaded in pGSNs is 52 % (ca. 1.08 $\mu g\,\mu g^{-1}$ pGSNs), while for SNs without a gold shell this value is 32 % (ca. 0.48 $\mu g\,\mu g^{-1}$ SNs). The cumulative DOC release profile (Figure S5 in the Supporting Information) shows an initial rapid release rate in 1–20 hours, and further sustained release with a lower release rate from 20 hours to 7 days. Over 60 % of the drug is released within 1 week. No obvious DOC cumulative release triggered by external NIR laser light was observed like in other reports.[14,15] This is attributable mainly to the good thermal and mechanical stability of pGSNs.

Internalization of nanoparticles into cells with high efficiency is important in drug delivery. For intracellular trafficking, luminescent-dye-loaded pGSNs were synthesized by incorporating the red fluorescent dye rhodamine B (RhB). After 2 hours of incubation, human liver carcinoma (HepG2) cells treated with pGSNs–RhB showed a strong red fluorescence signal throughout the entire cell cytoplasm. Some spots with higher fluorescence intensities resulting from aggregation of pGSNs demonstrated that the nanoparticles were localized in the cytoplasm after internalization (Figure S6a–c in the Supporting Information). This finding suggests that pGSNs can act as a transmembrane delivery carrier to increase cell internalization, decrease the drug efflux, and then increase the drug intracellular accumulation.[16]

DOC has been reported to have a hyperthermia-enhanced cytotoxicity.[17] To evaluate and compare the in vitro cytotoxicity of the free DOC, pGSNs, and pGSNs loaded with DOC (termed pGSNs-DOC) under irradiation by NIR light, the viability of cells was determined by using the 3-(4,5-dimethylthiazol-2-yl)-2,5-diphenyltetrazolium bromide (MTT) assay. HepG2 cells were incubated for 24 hours with a series of equivalent concentrations of free DOC dissolved in dimethyl sulfoxide and pGSNs-DOC. The pGSNs group had an equivalent Au dosage to the pGSNs-DOC group, and both groups were irradiated by NIR light (2 $W cm^{-2}$, 3 min). As seen from Figure 3a, with an increase of concentration all

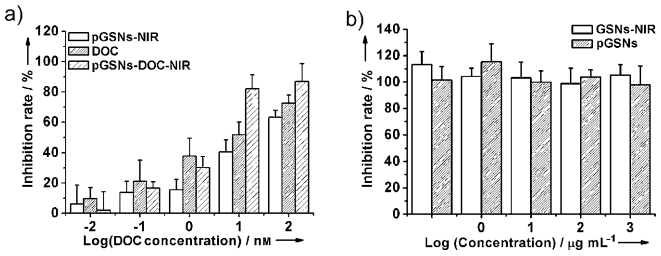

Figure 3. a) Inhibition rate of pGSNs, DOC, and pGSNs-DOC for 24 h as a function of DOC concentration. HepG2 cells were either not exposed to NIR light or irradiated with NIR light (2 $W cm^{-2}$ for 3 min). b) Viability of HepG2 cells with different concentrations of GSNs and pGSNs. Data represent the mean ± standard deviation of triplicate experiments.

three therapies show an increasing cytotoxicity against HepG2 cells in a dose-dependent manner. At a DOC concentration of 1 nM, the inhibition rate of free DOC was 37.8%, which indicates higher cytotoxicity than pGSNs–NIR (15.5%) and pGSNs-DOC–NIR (30.1%). The lower cell-killing potency with pGSNs-DOC–NIR could be attributed to the delayed DOC release from pGSNs in cells, and the relatively low concentration of pGSNs not producing enough heat to kill cells. At an equivalent DOC concentration of 10 nM, pGSNs-DOC–NIR shows a significantly enhanced cell-killing effect towards HepG2 cells with about 82.1% inhibition rate; in comparison, HepG2 cells treated with free DOC were 51.8% killed and HepG2 cells treated with pGSNs under NIR laser irradiation were only 40.5% killed. This inhibition rate is also higher than that of 100 nM free DOC.

Chemotherapeutics generally show a delicate balance between maintaining a high enough dose to kill cancer cells while avoiding a dose so high that it causes severe toxic effects.[18] So the synergistic effect of pGSNs-DOC–NIR is very attractive. The mechanism is speculated to be caused by the altered kinetics, permeability, and uptake of the chemotherapeutic agents during the heating process.[8] Given that no cytotoxicity is shown in the range from 0.1 to 1000 $\mu g mL^{-1}$ (Figure 3b), GSNs are promising in the expansion of the dosing range of chemotherapeutic drugs and in rendering patients safe cancer treatment. Additionally, by staining with the DNA-binding fluorophore Hoechst 33342 and propidium iodide under identical incubation conditions, we can observe the typical apoptotic condensation and fragmentation of chromatin for HepG2 cells treated with DOC and pGSNs-DOC–NIR, and there are also necrotic cells in these two groups. Fewer apoptotic and necrotic cells were observed in the group treated with pGSNs combined with NIR light than in the pGSNs-DOC–NIR group. There was no obvious cell damage without pGSNs nanoparticles under 2 $W cm^{-2}$ laser irradiation compared with a control group (Figure S7 in the Supporting Information). This result proves that pGSNs-DOC under NIR light irradiation can cause cell death by both apoptosis and necrosis.

Because the complicated in vivo environment could not be totally mimicked, it is important to evaluate the efficacy of in vivo therapy before clinical trials in humans. In this study, 15 female tumor burden ICR mice of H22 subcutaneous model were randomly distributed into three groups ($n = 5$): 1) treatment group, 2) Taxotere group, and 3) control group. The mice received intravenous (i.v.) treatment through the tail vein every 4 days a total of four times (days 1, 5, 9, and 13). At each time point for each treatment, a dosage of 20 $mg kg^{-1}$ DOC (200 μL for each mouse) was injected into the treatment and Taxotere groups. We hypothesize that a prolonged circulation time, in the size range of the effective enhanced permeability and retention (EPR) effect, would primarily affect the in vivo behavior of pGSNs for passive targeting in tumor sites while decreasing accumulation in other tissues.[19] Six hours after pGSNs-DOC injection, which allowed the systemically delivered pGSNs to accumulate in tumors, the tumors of the treatment group were irradiated for 3 minutes with NIR light under a laser power density of 2 $W cm^{-2}$. The control group received physiological saline (200 μL) without any irradiation. No mice died during the course of therapy. At day 17, mice were sacrificed and tumors were excised and weighed.

The tumor weights of the group treated by pGSNs-DOC were significantly lower than those of the control group with an average inhibition rate of 85.4%, which was also higher than the inhibition rate of the Taxotere group (57.4%; Figure 4). The mean tumor volumes and mean body weights in each group during the treatment are shown in Figures S8 and S9 in the Supporting Information. For the biodistribution study, mice bearing H22 tumors were intravenously injected with pGSNs at a dosage of 18.5 $mg kg^{-1}$ and sacrificed at 1, 6, 24, or 48 hours. TEM observation (Figure S10 in the Supporting Information) and inductively coupled plasma optical emission spectroscopy (ICP-OES; Figure S11 in the Support-

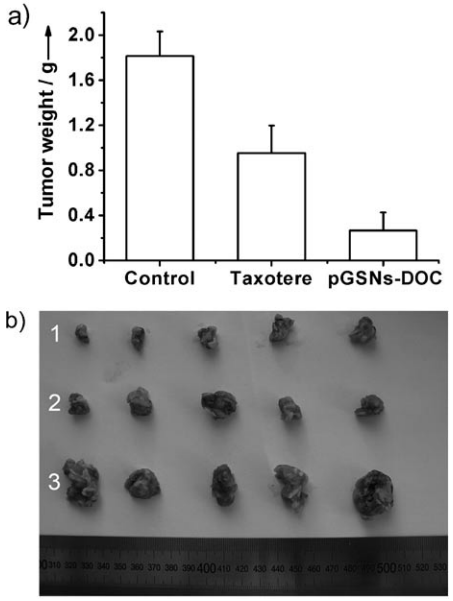

Figure 4. a) Tumor weights of each group after excision. b) Photograph of tumors from 1) pGSNs-DOC group, 2) Taxotere group, and 3) control group.

ing Information) both suggest the preferential accumulation of pGSNs in subcutaneous tumors in mice. As previously reported, local hyperthermia demonstrated a synergistic cell-killing therapy for the treatment of many solid tumors when used in combination with chemotherapy.[20] Furthermore, certain types of nanoparticles showed an interesting capacity to reverse multidrug resistance, which is a major problem in chemotherapy. Besides this, because of the EPR effect, nanoparticles can act as drug-delivery vectors which results in more drug loaded at the tumor site, thus improving cancer therapy and reducing the harmful nonspecific side effects of chemotherapeutics.[21] So the combination of thermal energy and chemotherapy offers many advantages over chemotherapy alone.

To access the effect of pGSNs as a drug carrier for reducing the toxicity of Taxotere, the systematic toxicity of Taxotere and pGSNs-DOC was evaluated in normal mice without tumors. Eighteen female ICR mice were randomly divided into three groups: a pGSNs-DOC group (20 mg kg^{-1} of DOC), Taxotere group (20 mg kg^{-1}), and control group (200 μL physiological saline). Intravenous administration was performed a total of three times in 9 days (days 1, 5, and 9). We assessed the systematic toxicity mainly from the loss of body weight, morphological and pathological examinations, hematology analysis, and blood biochemical assay. The mice in the Taxotere group lost an average of about 14% in weight, thus indicating toxicity compared with mice in the control and pGSNs-DOC groups, which showed an increase in body weight of 18 and 8%, respectively. The viscera indexes of the pGSNs-DOC and Taxotere groups showed no obvious change except that the viscera index of liver decreased for the Taxotere group, thus demonstrating liver damage (Figure S12 in the Supporting Information). This finding is consistent with the histological section of tissue samples stained with hematoxylin and eosin (H&E). No histopathological abnormities or lesions occurred in other organs of the pGSNs-DOC and Taxotere groups except for serious microgranuloma in the livers of the Taxotere group (Figure S13 in the Supporting Information).

For hematology analysis and blood biochemical assay, the absolute white blood cell count (WBC), granulocyte (GR), and monocyte (MO) decrease in the Taxotere group represent severe hematological toxicity (Table S3 in the Supporting Information). Compared with Taxotere, pGSN-DOC has reduced toxicity. Other hematological markers including mean corpuscular volume (MCV), mean corpuscular hemoglobin (MCH), mean corpuscular hemoglobin concentration (MCHC), and mean platelet volume (MPV) showed no obvious differences among the three groups. The increase of alanine aminotransferase (ALT) and aspartate aminotransferase (AST) indicates severe liver toxicity in the Taxotere group. Both Taxotere and pGSN-DOC have no obvious adverse influence on the plasma creatinine (CRE) and urea nitrogen (BUN) that represent kidney function. No statistically significant difference among the three groups was observed in other blood biochemical parameters. These data not only prove pGSNs as a drug vehicle can reduce the toxicity of the free drug, but also support the hypothesis that the EPR effect would help the enhanced accumulation of pGSNs in tumors rather than other tissues.

In summary, we have synthesized innovative multifunctional GSNs, which can combine remote-controlled photothermal therapy with chemotherapy like a "magic bullet". They also reduce drug side effects by sustained drug release and provide a new multimodality cancer treatment with higher efficacy and less toxicity than the free drug. Last but not least, we still need to optimize the photothermal therapy and chemotherapy process, and quantify the tissue injury. Moreover, the mechanism of combination of the two therapies is still not completely understood. Whether increasing the temperature also induces immunological changes (for instance, the release of heat shock proteins and subsequently maybe an improved immune recognition) is totally unknown and worth investigating.[22] Although there are many unsolved problems, we still expect that the combination of the unique structural characteristics and integrated functions of multicomponent gold nanoshells will attract increasing research interest and could lead to new opportunities in nanomedicine.

Received: May 10, 2010
Revised: June 21, 2010
Published online: November 25, 2010

Keywords: antitumor agents · chemotherapy · drug delivery · nanomedicine · photothermal therapy

[1] L. R. Hirsch, R. J. Stafford, J. A. Bankson, S. R. Sershen, B. Rivera, R. E. Price, J. D. Hazle, N. J. Halas, J. L. West, *Proc. Natl. Acad. Sci. USA* **2003**, *100*, 13549–13554.

[2] a) X. H. Huang, I. H. El-Sayed, Q. Wei, M. A. El-Sayed, *J. Am. Chem. Soc.* **2006**, *128*, 2115–2120; b) W. S. Kuo, C. N. Chang, Y. T. Chang, M. H. Yang, Y. H. Chien, S. J. Chen, C. S. Yeh,

Angew. Chem. **2010**, *122*, 2771 – 2775; *Angew. Chem. Int. Ed.* **2010**, *49*, 2711 – 2715.
[3] J. Y. Chen, C. Glaus, R. Laforest, Q. Zhang, M. X. Yang, M. Gidding, M. J. Welch, Y. N. Xia, *Small* **2010**, *6*, 811 – 817.
[4] K. W. Hu, C. C. Huang, J. R. Hwu, W. C. Su, D. B. Shieh, C. S. Yeh, *Chem. Eur. J.* **2008**, *14*, 2956 – 2964.
[5] H. Y. Liu, D. Chen, F. Q. Tang, G. J. Du, L. L. Li, X. W. Meng, W. Liang, Y. E. Zhang, X. Teng, Y. Li, *Nanotechnology* **2008**, *19*, 455101.
[6] S. T. Wang, K. J. Chen, T. H. Wu, H. Wang, W. Y. Lin, M. Ohashi, P. Y. Chiou, H. R. Tseng, *Angew. Chem.* **2010**, *122*, 3865 – 3869; *Angew. Chem. Int. Ed.* **2010**, *49*, 3777 – 3781.
[7] a) J. Kim, S. Park, J. E. Lee, S. M. Jin, J. H. Lee, I. S. Lee, I. Yang, J. S. Kim, S. K. Kim, M. H. Cho, T. Hyeon, *Angew. Chem.* **2006**, *118*, 7918 – 7922; *Angew. Chem. Int. Ed.* **2006**, *45*, 7754 – 7758; b) J. Kim, J. E. Lee, J. Lee, Y. Jang, S. W. Kim, K. An, J. H. Yu, T. Hyeon, *Angew. Chem.* **2006**, *118*, 4907 – 4911; *Angew. Chem. Int. Ed.* **2006**, *45*, 4789 – 4793; c) H. Y. Park, J. Yang, J. Lee, S. Haam, I. H. Cho, K. H. Yoo, *ACS Nano* **2009**, *3*, 2919 – 2926; d) L. L. Ma, M. D. Feldman, J. M. Tam, A. S. Paranjape, K. K. Cheruku, T. A. Larson, J. O. Tam, D. R. Ingram, V. Paramita, J. W. Villard, J. T. Jenkins, T. Wang, G. D. Clarke, R. Asmis, K. Sokolov, B. Chandrasekar, T. E. Milner, K. P. Johnston, *ACS Nano* **2009**, *3*, 2686 – 2696; e) C. G. Wang, J. Irudayaraj, *Small* **2010**, *6*, 283 – 289; f) C. G. Wang, J. J. Chen, T. Talavage, J. Irudayaraj, *Angew. Chem.* **2009**, *121*, 2797 – 2801; *Angew. Chem. Int. Ed.* **2009**, *48*, 2759 – 2763; g) L. Y. Wang, J. W. Bai, Y. J. Li, Y. Huang, *Angew. Chem.* **2008**, *120*, 2473 – 2476; *Angew. Chem. Int. Ed.* **2008**, *47*, 2439 – 2442.
[8] T. S. Hauck, T. L. Jennings, T. Yatsenko, J. C. Kumaradas, W. C. W. Chan, *Adv. Mater.* **2008**, *20*, 3832 – 3838.
[9] D. Chen, L. L. Li, F. Q. Tang, S. Qi, *Adv. Mater.* **2009**, *21*, 3804 – 3807.
[10] S. J. Oldenburg, R. D. Averitt, S. L. Westcott, N. J. Halas, *Chem. Phys. Lett.* **1998**, *288*, 243 – 247.
[11] Y. Xia, N. J. Halas, *MRS Bull.* **2005**, *30*, 338 – 348.
[12] a) D. A. Giljohann, D. S. Seferos, W. L. Daniel, M. D. Massich, P. C. Patel, C. A. Mirkin, *Angew. Chem.* **2010**, *122*, 3352 – 3366; *Angew. Chem. Int. Ed.* **2010**, *49*, 3280 – 3294; b) D. P. O'Neal, L. R. Hirsch, N. J. Halas, J. D. Paynea, J. L. West, *Cancer Lett.* **2004**, *209*, 171 – 176.
[13] S. Link, M. A. El-Sayed, *Int. Rev. Phys. Chem.* **2000**, *19*, 409 – 453.
[14] H. Park, J. Yang, S. Seo, K. Kim, J. Suh, D. Kim, S. Haam, K. H. Yoo, *Small* **2008**, *4*, 192 – 196.
[15] J. You, G. D. Zhang, C. Li, *ACS Nano* **2010**, *4*, 1033 – 1041.
[16] M. M. Gottesman, T. Fojo, S. E. Bates, *Nat. Rev. Cancer* **2002**, *2*, 48 – 58.
[17] F. Mohamed1, P. Marchettini1, O. A. Stuart, M. Urano, P. H. Sugarbaker1, *Ann. Surgical Oncol.* **2003**, *10*, 463 – 468.
[18] A. Felici, J. Verweij, A. Sparreboom, *Eur. J. Cancer* **2002**, *38*, 1677 – 1684.
[19] J. Huwyler, J. Drewe, S. Krähenbüh, *Int. J. Nanomed.* **2008**, *3*, 21 – 29.
[20] a) K. Komatsu, R. C. Miller, E. J. Hall, *Br. J. Cancer* **1988**, *57*, 59 – 63; b) K. Nakajima, H. Hisazumi, *Urol. Res.* **1987**, *15*, 255 – 260.
[21] L. E. van Vlerken, M. M. Amiji, *Expert Opin. Drug Delivery* **2006**, *3*, 205 – 216.
[22] A. G. van der Heijden, L. A. Kiemeney, O. N. Gofrit, O. Nativ, A. Sidi, Z. Leib, R. Colombo, R. Naspro, M. Pavone, J. Baniel, F. Hasner, J. A. Witjes, *Eur. Urol.* **2004**, *46*, 65 – 72.

